

Studies of backward particle production with A Fixed-Target Experiment using the LHC beams

Federico Alberto Ceccopieri*

*IFPA, Université de Liège, Allée du 6 août,
B4000, Liège, Belgium*

The foreseen capability to cover the far backward region at A Fixed-Target Experiment using the LHC beams allows to explore the dynamics of target fragmentation in hadronic collisions. In this report we briefly outline the required theoretical framework and discuss a number of studies of forward and backward particle production. By comparing this knowledge with the one accumulated in Deep Inelastic Scattering on target fragmentation, the basic concept of QCD factorisation could be investigated in detail.

Keywords: Fracture Functions, Target fragmentation, Evolution, Factorisation

I. INTRODUCTION

In hadronic collisions a portion of the produced particle spectrum is characterised by hadrons carrying a sizeable fraction of the available centre-of-mass energy, the so-called leading particle effect. It is phenomenologically observed that for such hadrons their valence-parton composition is almost or totally conserved with respect to the one of initial-state hadrons [1]. In pp collisions, for example, protons, neutrons and lambdas show a significant leading particle effect. Moreover, for such semi-inclusive processes, the production cross section peaks at very small transverse momenta with respect to the collision axis, a regime where perturbative techniques can not be applied, giving insight on non-perturbative aspects of QCD dynamics in high energy collisions.

Quite interestingly, the leading particle effect has been observed in Semi-Inclusive Deep Inelastic Scattering (SIDIS). At variance with the hadronic processes mentioned above, such

*Electronic address: federico.alberto.ceccopieri@cern.ch

a process naturally involves a large momentum transfer. The presence of a hard scale enables the derivation of a dedicated factorisation theorem [2, 3] which ensures that QCD factorisation holds for backward particle production in DIS. The relevant cross sections can then be factorised into perturbatively calculable short-distance cross sections and new distributions, fracture functions, which simultaneously encode information both on the interacting parton and on the spectator fragmentation into the observed hadron. Despite of being non-perturbative in nature, their scale dependence can be calculated within perturbative QCD [4]. The factorisation theorem [2, 3] guarantees that fracture functions are universal distributions, at least in the context of SIDIS.

Detailed experimental studies of hard diffraction at HERA have shown to support the hypothesis of QCD factorisation and evolution inherent the fracture functions formalism. Furthermore they led to a quite accurate knowledge of diffractive parton distributions [5–8], a special case of fracture functions in the very backward kinematic limit. For particles other than protons, proton-to-neutron fracture functions have been extracted from a pQCD analysis of forward neutron production in DIS in Ref. [9]. A set of proton-to-lambda fracture functions has been obtained by performing a combined pQCD fit to a variety of semi-inclusive DIS lambda production data in Ref. [10].

As theoretically anticipated in Ref. [2, 11, 12] and experimentally observed in hard diffraction in $p\bar{p}$ collisions at Tevatron [13, 14], QCD factorisation is violated for fracture functions in hadronic collisions. On general grounds, it might be expected, in fact, that the dynamics of target-remnants hadronisation is affected by the coloured environment resulting from the scattering in a rather different way with respect to the Deep Inelastic Scattering case.

Nonetheless, the tools mentioned above allow to investigate quantitatively particle production mechanisms in the very backward and forward regions, to test the concept of factorisation at the heart of QCD and to study the dependencies of factorisation breaking upon the species and the kinematics of the selected final state particle.

This physics program could be successfully carried on at A Fixed-Target Experiment using the LHC beams [15]. Novel experimental techniques are, in fact, available to extract beam-halo protons or heavy-ions from LHC beams without affecting LHC performances. Such a resulting beam would be then impinged on a high-density and/or long-length fixed target, guaranteeing high luminosities. Furthermore and most importantly for the physics program to be discussed here, the entire backward hemisphere (in the centre-of-mass system

of the collision) would be accessible with standard experimental techniques allowing high precision studies of target fragmentation. Although measurements of particle production in the very forward region (close to the beam axis) might be challenging experimentally due to the high particle densities and large energy flow, the installation of dedicated detectors, like forward neutron calorimeters and/or proton taggers, could further broaden the physics program outlined above giving access to the beam fragmentation region.

The paper is organised as follows. In Sec. II we first give a brief theoretical introduction on the fracture functions formalism and to higher order corrections to the semi-inclusive Drell-Yan process. In Sec. III we outline different analyses which could be performed at AFTER@LHC with special focus on single hard diffraction. In Sec. IV we summarise our results.

II. COLLINEAR FACTORISATION FORMULA

Fracture functions, originally introduced in DIS, do depend on a large momentum transfer. Therefore, in order to use them in hadronic collisions, a hard process must be selected. We consider here the semi-inclusive version of the Drell-Yan process,

$$H_1(P_1) + H_2(P_2) \rightarrow H(h) + \gamma^*(q) + X, \quad (1)$$

in which one hadron H is measured in the final state together with a Drell-Yan pair. In such a process the high invariant mass of the lepton pair, $q^2 = Q^2$, allows the applicability of perturbative QCD, while the detected hadron H can be used, without any phase space restriction, as a local probe to investigate particle production mechanisms.

The associated production of a particle and a Drell-Yan pair in terms of partonic degrees of freedom starts at $\mathcal{O}(\alpha_s)$. One of the contributing diagrams is depicted in Fig. (1). Assuming that the hadronic cross-sections admit a factorisation in terms of long distance non-perturbative distributions and short distance perturbative calculable matrix elements for the partonic process $i(p_1) + j(p_2) \rightarrow l(k) + \gamma^*(q)$, predictions based on perturbative QCD are obtained convoluting the relevant partonic sub-process cross-sections, $d\hat{\sigma}^{ij \rightarrow l\gamma^*}$, with parton distribution functions, f_{i/H_1} and f_{j/H_2} , and fragmentation functions, $D^{H/l}$. The hadronic cross section, at centre of mass energy squared $s = (P_1 + P_2)^2$, can be symbolically

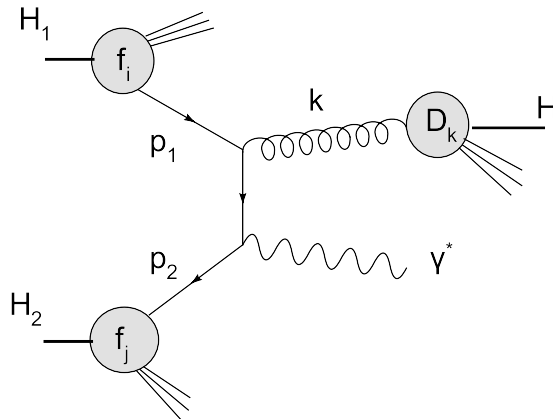


FIG. 1: Example of diagram contributing to hadron production in the central fragmentation region to order $\mathcal{O}(\alpha_s)$ in eq.(2).

written as [16, 17]

$$\frac{d\sigma^{H,C,(1)}}{dQ^2 dz} \propto \sum_{i,j,l} \int \frac{dx_1}{x_1} \int \frac{dx_2}{x_2} \int \frac{d\rho}{\rho} f_i^{[1]}(x_1) f_j^{[2]}(x_2) D^{H/l}(z/\rho) \frac{d\hat{\sigma}^{ij \rightarrow l\gamma^*}}{dQ^2 d\rho}, \quad (2)$$

where the convolutions are over the momentum fractions of the incoming and outgoing partons. The partonic indices i , j and l in the sum run on the available partonic subprocesses. The superscripts label the incoming hadrons and the presence of crossed terms is understood. This type of factorised hadronic cross section is expected to hold for hadrons produced at sufficiently high transverse momentum and it is widely and successfully used to compute cross sections for large momentum transfer processes in hadronic collisions. The Lorentz-invariant variable z in eq. (2) is defined by

$$z = \frac{2h \cdot (P_1 + P_2)}{s} \equiv \frac{2E_H^*}{\sqrt{s}}. \quad (3)$$

In the hadronic centre-of-mass frame, where the second identity holds, z is just the observed hadron energy, E_H^* , scaled down by the beam energy $\sqrt{s}/2$. The variable ρ , appearing in eq. (2), is its partonic equivalent. Within this production mechanism, the observed hadron H is generated by the fragmentation of the final state parton l , and for this reason we address it as *central*. The amplitudes squared [18], however, are singular when the transverse momentum of the final state parton vanishes. In such configurations, the parent parton l of the observed hadron H is collinear either to the incoming parton i or j . As these phase space region are approached, perturbation theory loses its predictivity. This class of

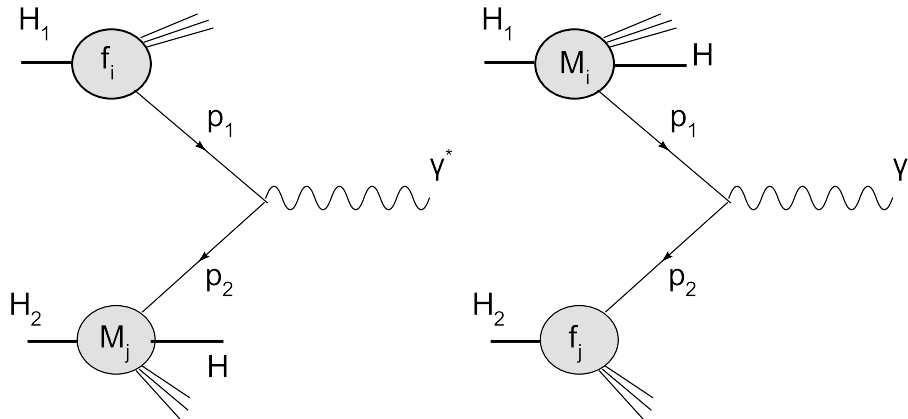


FIG. 2: Pictorial representation of the parton model formula, eq. (4), for the associated production of a Drell-Yan pair and a particle in the target fragmentation regions.

collinear singularities escape the usual renormalisation procedure which amounts to reabsorb collinear divergences into a redefinition of bare parton distribution and fragmentation functions. Such singularities are likely to appear in every fixed order calculation in the same kinematical limits spoiling the convergence of the perturbative series. In Refs [16, 17] a generalised procedure for the factorisation of such additional collinear singularities is proposed. The latter is the same as the one proposed in Deep Inelastic Scattering [19] where the same singularities pattern is also found, confirming the universality of collinear radiation between different hard processes. Such a generalised collinear factorisation makes use of fracture functions. These distributions obey DGLAP-type evolution equations which contain an additional inhomogeneous term resulting from the subtraction of collinear singularities in the target-fragmentation region [4, 19]. Such equations allow to resum the corresponding large logarithmic corrections to all orders in perturbation theory. Bare fracture functions, $M_i^{H/H_1}(x, z)$, describe the hadronization of the spectators system in hadron-induced reactions. They express the conditional probability to find a parton i entering the hard scattering while an hadron H is produced with fractional momentum z in the target fragmentation region of the incoming hadron H_1 .

The use of fracture functions allows particle production already to $\mathcal{O}(\alpha_s^0)$, since the hadron H can be non-perturbatively produced by a fracture function itself. Therefore the lowest order parton model formula can be symbolically written as

$$\frac{d\sigma^{H,T,(0)}}{dQ^2 dz} \propto \sum_{i,j} \int \frac{dx_1}{x_1} \int \frac{dx_2}{x_2} [M_i^{[1]}(x_1, z) f_j^{[2]}(x_2) + M_i^{[2]}(x_2, z) f_j^{[1]}(x_1)] \frac{d\hat{\sigma}^{ij \rightarrow \gamma^*}}{dQ^2} \quad (4)$$

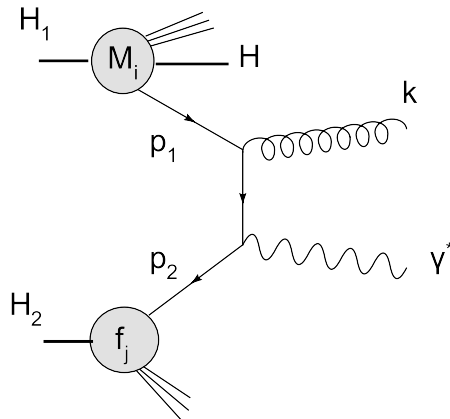


FIG. 3: *Example of diagram contributing to $\mathcal{O}(\alpha_s)$ corrections in the target fragmentation region, eq.(5).*

and it is sketched in Fig. (2). The superscripts in eq. (4) indicate from which incoming hadron, H_1 or H_2 , the outgoing hadron H is produced through a fracture functions. In order to complete the calculation to $\mathcal{O}(\alpha_s)$ accuracy we should consider higher order corrections to eq. (4). Since in this case the hadron H is already produced by fracture functions, final state parton radiation should be integrated over and the resulting contribution added to virtual corrections. One of the contributing diagrams is depicted in Fig. (3). The general structure of these terms is

$$\frac{d\sigma^{H,T,(1)}}{dQ^2 dz} \propto \sum_{i,j} \int \frac{dx_1}{x_1} \int \frac{dx_2}{x_2} [M_i^{[1]}(x_1, z) f_j^{[2]}(x_2) + M_i^{[2]}(x_2, z) f_j^{[1]}(x_1)] \frac{d\hat{\sigma}^{ij \rightarrow (l)\gamma^*}}{dQ^2}. \quad (5)$$

We refer to them as to the *target* fragmentation contributions. Their calculation is, a part from minor differences in kinematics, completely analogous to the one of the inclusive Drell-Yan case. The factorisation procedure, first elaborated in Ref. [19] in the context of SIDIS, amounts to substitute in eq. (4) the bare fracture and parton distributions functions with their renormalised version [16, 17]. Renormalised parton distributions and fracture functions homogeneous terms do cancel, as in the inclusive Drell-Yan case, all singularities present in eq. (5). The additional singularities in eq. (2) are cancelled by the combination of parton distributions and fracture functions inhomogeneous renormalisation terms. Adding all the various contributions, the resulting hadron- p_t integrated cross section, up to order $\mathcal{O}(\alpha_s)$, is

then infrared finite [16, 17] and can be symbolically written as

$$\frac{d\sigma^H}{dQ^2 dz} \propto \frac{\sigma_0}{N_c s} \sum_{i,j} [M_i^{[1]} \otimes f_j^{[2]} + M_i^{[2]} \otimes f_j^{[1]}] \left(1 + \frac{\alpha_s}{2\pi} C^{ij}\right) + \frac{\sigma_0}{N_c s} \frac{\alpha_s}{2\pi} \sum_{i,j,l} f_i^{[1]} \otimes f_j^{[2]} \otimes D^{H/l} \otimes K_l^{ij}, \quad (6)$$

where $\sigma_0 = 4\pi\alpha_{em}^2/3Q^2$ and N_c is the number of colors. We refer to the previous equation as to the collinear factorisation formula for the process under study. The next-to-leading order coefficients C^{ij} and K_l^{ij} have been calculated in Ref. [17], making the whole calculation ready for numerical implementation.

We stress, however, that our ability to consistently subtract collinear singularities in such a semi-inclusive process is a necessary but not sufficient condition for factorisation to hold in hadronic collisions. The one-loop calculation outlined above in fact does involve only the so-called active partons. It completely ignores multiple soft parton exchanges between active and spectators partons, whose effects should be accounted for in any proof of QCD factorisation. Therefore there is no guarantee that fracture functions extracted from SIDIS can be successfully used to describe forward or backward particle production in hadronic collisions. Reversing the argument, such a comparison may instead offer new insights on non-perturbative aspects of QCD and to the breaking of factorisation.

III. SINGLE HARD DIFFRACTION AT AFTER@LHC

As an application of the formalism presented in the previous sections we will consider single hard diffractive production of a Drell-Yan pair

$$p_1(P_1) + p_2(P_2) \rightarrow p(P) + \gamma^*(q) + X, \quad (7)$$

where we have indicated in parathesis the four momenta of the relevant particles. We present in the following cross sections differential in the virtual photon variables. The subsequent decay of the virtual photon into a lepton pair can be easily included so that realistic cuts on leptons rapidity and transverse momentum can then be applied. We consider the AFTER@LHC kinematic setting in which a 7 TeV proton beam collides on a fixed target proton leading to a centre-of-mass energy of $\sqrt{s} = 115$ GeV. We consider the projectile proton p_1 moving in the positive z direction and p_2 at rest in the laboratory. The diffractively

produced proton p has in general almost the incoming projectile proton p_1 energy and very small transverse momentum as measured with respect to the collision axis. The detection of such fast protons will in general require the installation of forward proton taggers. The lepton pair instead will be measured by the main AFTER@LHC detector. This kinematical configurations is pictorially represented in right plot of Fig. (2).

Diffraction processes has been intensively analysed in DIS at HERA ep collider, revealing their leading twist nature. From scaling violations of the diffractive structure functions [5, 8] and dijet production in the final state [6, 7] quite precise diffractive parton distributions functions (dPDFs) have been extracted from HERA data, which parametrise the parton content of the color singlet exchanged in the t -channel. The comparison of QCD predictions for single diffractive hard processes based on diffractive parton distributions measured at HERA against data measured at Tevatron [13, 14] ($\sqrt{s} = 1.96$ TeV), adopting a factorised ansatz as in eq. (4), has indeed revealed that these processes are, not unexpectedly [11, 12], significantly suppressed in hadronic collisions. This conclusion persists even after the inclusion of higher order QCD corrections [20]. Complementing these results with the forthcoming ones at LHC at higher at $\sqrt{s} = 13$ TeV and the ones from AFTER@LHC at $\sqrt{s} = 115$ GeV will give insight on the energy dependence of the so-called rapidity gap survival (RGS) probability in a wide range in \sqrt{s} . Since the theoretical computation of the RGS factor is highly model dependent, we decided not to include it in our predicted cross sections which must be considered therefore as upper bounds.

Diffractive parton distributions f_i^D are in general proton-to-proton fracture functions M_i . They depend upon the final state proton fractional energy loss, $x_{IP} = 1 - z$ with z given in eq. (3), the fractional momentum of the interacting parton with respect to the pomeron momentum, $\beta = x/x_{IP}$ and the virtuality Q^2 . In general fracture functions may depend also upon the invariant momentum transfer $t = (P - P_1)^2$ at the proton vertex [21]. In all diffractive structure functions measurements at HERA, out of which dPDFs are determined, t is integrated over up to some $t^{max} \ll Q^2$. In this case dPDFs obey ordinary DGLAP evolution equations [22] as their extended, t -dependent, version [21]. In the present paper we use dPDFs from Ref. [5] which are defined by $|t| < 1$ GeV². Since they are extracted from large rapidity gap data where the proton is not directly measured, they contain a contribution (23%) from the so-called proton dissociation contribution. In order to use

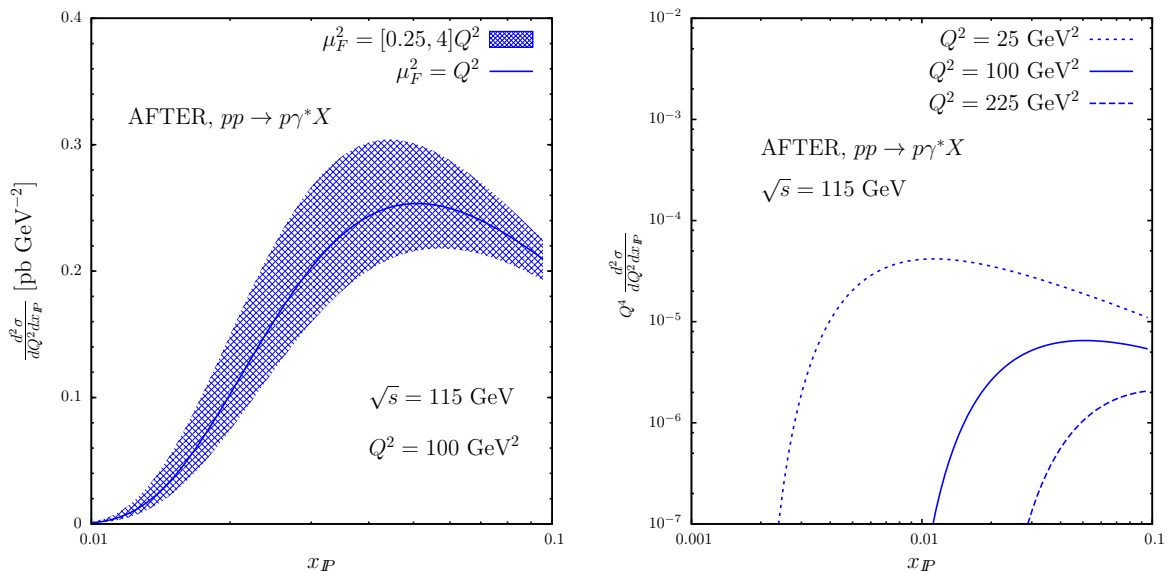


FIG. 4: *Left:* Double differential cross sections for the production of a Drell-Yan pair of mass $Q^2 = 100 \text{ GeV}^2$. Blue error bands represent theoretical errors estimation, as described in the text. *Right:* Double differential cross sections times Q^4 for three different invariant masses.

dPDFs in the present context we first note that

$$M_i(x_1, z, Q^2) = x_{IP}^{-1} f_i^D(\beta, x_{IP}, Q^2). \quad (8)$$

The extra factor x_{IP}^{-1} comes from the jacobian of the change $x_1 = \beta x_{IP}$. We then rearrange eq. (4) in terms of new variables obtaining

$$\frac{d\sigma^D}{dQ^2 dx_{IP}} = \frac{\sigma_0}{N_c s} \int_{\tau/\beta}^1 \frac{d\beta}{\beta} \sum_{q, \bar{q}} e_q^2 x_{IP}^{-1} f_q^D(\beta, x_{IP}, \mu_F^2) f_{\bar{q}}\left(\frac{\tau}{\beta x_{IP}}, \mu_F^2\right), \quad (9)$$

with $\tau = Q^2/s$. For simplicity we consider here leading order formulas but the extension to higher order is straightforward. In eq. (9) we use parton distribution functions from Ref. [23]. We show explicitly the dependence of fracture and parton distributions functions upon the factorisation scale, μ_F^2 . Predictions are obtained with this scale set to $\mu_F^2 = Q^2$. Theoretical errors associated with higher order corrections are instead estimated varying such scale in the range $\mu_F^2 = 1/4Q^2$ and $\mu_F^2 = 4Q^2$.

In Fig. (4) we present predictions for the x_{IP} distribution. In left plot we consider a Drell-Yan pair of mass $Q^2 = 100 \text{ GeV}^2$. The distribution shrinks as lower x_{IP} -values are approached whereas, from hard diffraction at HERA, it is well known that diffractive cross sections rise as an inverse power of x_{IP} . Such effect therefore is then attributed to phase

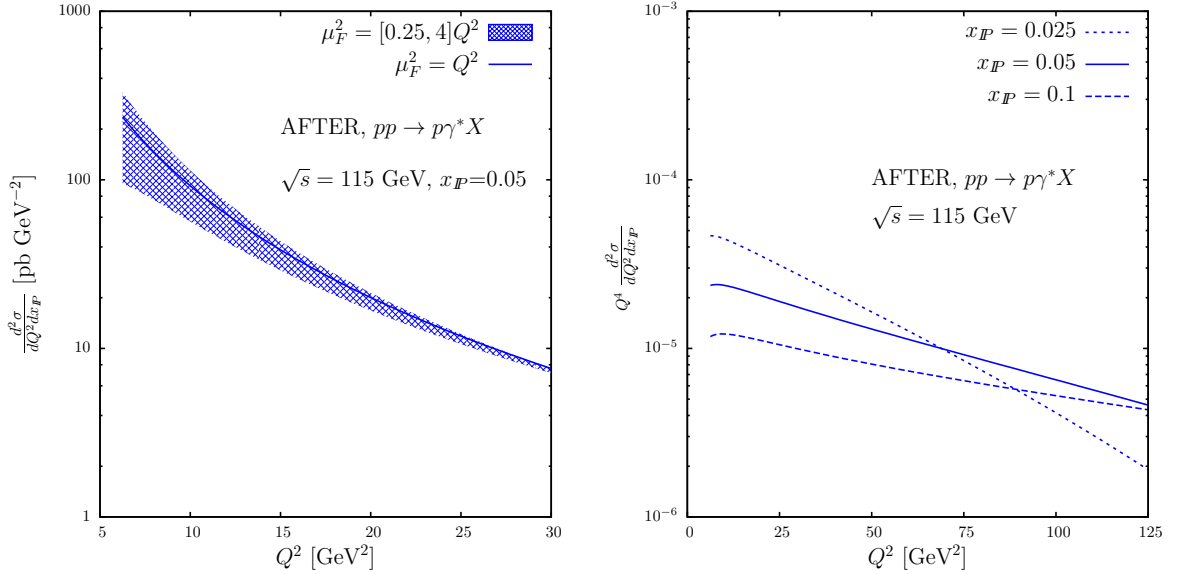


FIG. 5: *Left: Double differential cross sections for the production of a Drell-Yan pair at $x_{IP} = 0.05$. Blue error bands represent theoretical errors estimation, as described in the text. Right: Double differential cross sections times Q^4 for three different x_{IP} -values.*

space threshold effects. The Drell-Yan invariant mass constraint can be rewritten in the diffractive case as $Q^2 = \beta x_{IP} x_2 s$, which can be cast (for $\beta \rightarrow 1$ and $x_2 \rightarrow 1$) in upper bound on the invariant mass $Q^2 < x_{IP} s$ at fixed x_{IP} and s . This hypothesis is further supported in the right plot of Fig. (4), where differential distributions are presented for three values of Q^2 . The former is multiplied by Q^4 to compensate the fast fall off of the electromagnetic cross section. The lowest values of x_{IP} are then accessed only by lowering the invariant mass of the pair. We note that, even considering the maximum value of $x_{IP} = 0.1$, single diffractive production of W^\pm and Z is beyond the kinematic reach at AFTER@LHC. In the left panel of Fig. (5) we present the prediction for the Q^2 distribution at a fixed value of $x_{IP} = 0.05$. The cross section, as expected, is fast falling as an inverse power of Q^2 . The Q^2 distribution is particularly instructive since it allows to study the possible dependence of the RGS factor on Q^2 and therefore to determine the underlying dynamics. In the right panel of Fig. (5) we present the Q^2 -differential cross section again multiplied by the factor Q^4 . In this way all the Q^2 dependence is accounted for by that of fracture and parton distributions. These curves and the corresponding slopes, however, can not be readily interpreted as genuine results of QCD evolution of fracture and parton distributions functions because of the threshold effect mentioned above appearing at such moderate values of \sqrt{s} .

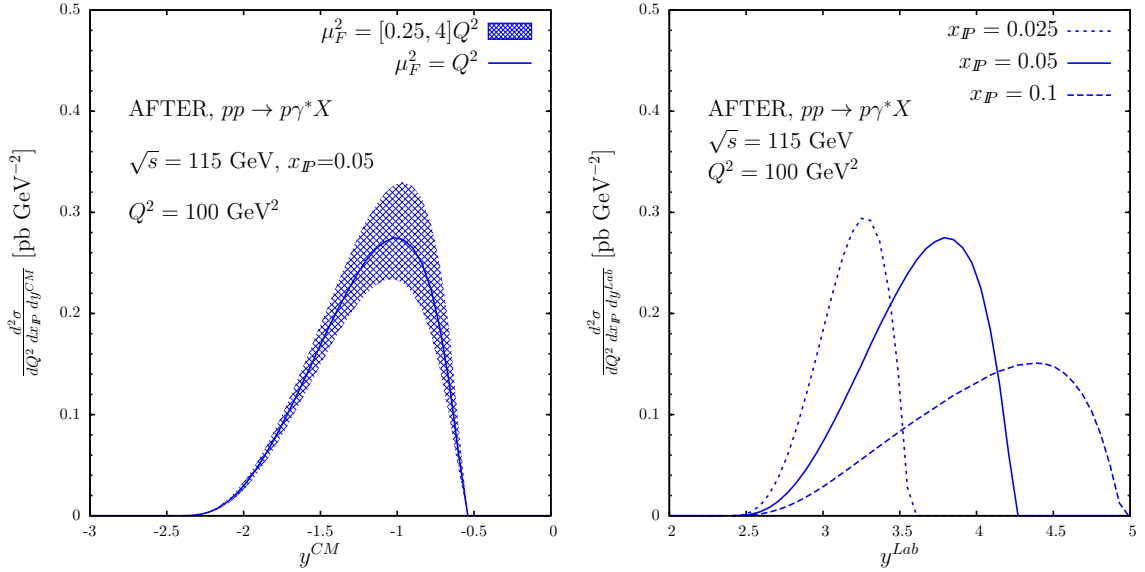


FIG. 6: *Left:* Triple differential cross sections for the production of a Drell-Yan pair at $x_{IP} = 0.05$ and of mass $Q^2 = 100 \text{ GeV}^2$. Blue error bands represent theoretical errors estimation, as described in the text. *Right:* Triple differential cross sections for three different x_{IP} -values.

By changing variable from β to the virtual photon centre-of-mass rapidity, y^{CM} ,

$$\beta = \frac{\sqrt{\tau}}{x_{IP}} e^{y^{CM}}, \quad x_2 = \sqrt{\tau} e^{-y^{CM}}, \quad (10)$$

eq. (9) can be further manipulated to give the three-differential cross section

$$\frac{d\sigma^D}{dQ^2 dx_{IP} dy^{CM}} = \frac{\sigma_0}{N_c s} \sum_{q, \bar{q}} e_q^2 x_{IP}^{-1} f_q^D(\beta, x_{IP}, \mu_F^2) f_{\bar{q}}(x_2, \mu_F^2). \quad (11)$$

The rapidity range for diffractive Drell-Yan production reads

$$\ln \sqrt{\tau} < y^{CM} < \ln \frac{\sqrt{\tau}}{x_{IP}} \quad (12)$$

which, as expected, turns out to be asymmetric given the kinematic constraint $x_1 < x_{IP}$. The rapidity range for the inclusive Drell-Yan case is recovered simply setting $x_{IP} = 1$. The rapidity distributions is particularly sensitive to the shape the diffractive parton distributions. This distribution will be useful to investigate any possible kinematic dependence of the RGS factor. In the left panel of Fig. (6) we present the centre-of-mass rapidity distribution at fixed $Q^2 = 100 \text{ GeV}^2$ and $x_{IP} = 0.05$. In this frame the distribution is shifted at negative values of y^{CM} . Therefore, on average, the parton originating from the target proton carries more momentum than the one originating from the pomeron. Since the rapidity is additive

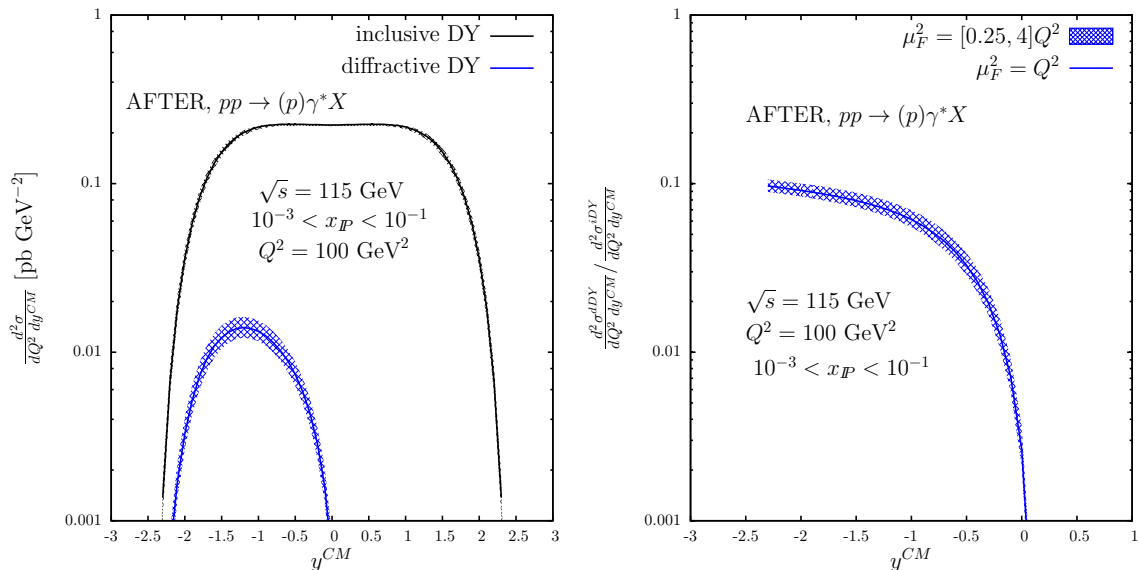


FIG. 7: *Left: Rapidity distributions for inclusive and diffractive Drell-Yan of mass $Q^2 = 100 \text{ GeV}^2$. Blue error bands represent theoretical errors estimation, as described in the text. Right: diffractive to inclusive Drell-Yan rapidity distributions ratio.*

under boost along the collision axis we may easily boost the y^{CM} to the laboratory frame by using

$$y^{Lab} = \frac{1+c}{1-c} + y^{CM} \quad \text{with} \quad c = \sqrt{1 - \frac{4m_p^2}{s}} \quad (13)$$

with m_p the proton mass. In the AFTER@LHC kinematics this implies a rapidity shift $\Delta y = y^{Lab} - y^{CM} = 4.8$. The rapidity distributions in the laboratory frame for a Drell-Yan pair of mass $Q^2 = 100 \text{ GeV}^2$ and for three different x_{IP} values are presented in the right panel of Fig. (6). One may notice from the plot that for increasing x_{IP} the Drell-Yan pair spans a wider rapidity range and the corresponding spectrum is increasingly more forward. It might be useful to discuss the single diffractive Drell-Yan pair production in conjunction with the analogous inclusive process. Such a comparison is presented for the centre-of-mass rapidity distributions in the left plot of Fig. (7) for a common Drell-Yan pair of mass squared $Q^2 = 100 \text{ GeV}^2$ and, for the diffractive case, integrated in the range $10^{-3} < x_{IP} < 10^{-1}$. The rapidity distributions in the single diffractive case is strongly asymmetric whereas in the inclusive case it is symmetric around $y^{CM} = 0$. This effect is primarily due to the different kinematics of the two processes and to the different fractional momentum distributions between parton and fracture distributions. In the right plot of Fig. (7) the ratio between the two previous distributions is presented. The ratio gives

direct information on the suppression factor between the single diffractive to the inclusive process, assuming a factorised expression for the former, eq. (11). Such ratio might be convenient from the experimental side since many lepton detection systematics will cancel. On the theoretical one it is expected to be more stable against the inclusion of higher order corrections. In the present case, for example, the factorisation scale is simultaneously varied both on the numerator and denominator resulting in a reduced theoretical error band with respect to the one obtained for absolute cross sections.

We wish to end this section with a brief overview of other possible applications of the proposed formalism. A completely analogous program can be performed for the associated production of forward neutron and a Drell-Yan pair, $p + p \rightarrow n + \gamma^* + X$. The production of forward neutron in DIS at HERA has shown a leading twist nature. From scaling violations of the semi-inclusive neutron structure functions a set of proton-to-neutron fracture functions set has been extracted from data in Ref. [9] which can be used to predict forward neutron rate in hadronic collisions. As in the case of hard diffraction, both physics programs would highly benefit from the installation of a dedicated instrumentation for the measurements of fast neutrons and protons quite close to the beam axis. Measurements in the forward region, although problematic experimentally, give in fact direct access to the study of the beam fragmentation region.

As a third application we consider hyperon production associated with a Drell-Yan pair, $p + p \rightarrow V + \gamma^* + X$, where V generically indicates either a Λ^0 or $\bar{\Lambda}^0$ hyperon. At very low transverse momentum, Λ^0 longitudinal momentum spectrum should show a significant leading particle effect, which can be predicted, assuming factorisation as in $d\sigma^{H,T}$, by the proton-to-lambda fracture functions set obtained from a fit to SIDIS data in Ref. [10]. On the other hand $\bar{\Lambda}^0$ spectrum in the same kinematical conditions should instead show almost no leading particle effect, giving access to the proton-to- $\bar{\Lambda}^0$ fracture functions. We note, in general, that the particle-to-antiparticle fracture function is indeed an interesting and almost unknown distribution. On the other hand, if one considers Λ^0 or $\bar{\Lambda}^0$ at sufficiently large transverse momentum, their combined analysis, described by $d\sigma^{H,C}$, should allow the investigation of parton hadronisation into hyperons in the QCD vacuum as parametrised by fragmentation functions.

As a last application we consider the associated production of one particle and a Drell-Yan pair in the context of multi-parton interactions. The latter process has already been used to

investigate the contamination of the so-called underlying event [24] to jet observable and has been successfully used to study underlying event properties [25]. If the detected hadron is measured at sufficiently large transverse momentum, the latter constitutes a natural infrared regulator for the partonic matrix elements. In this kinematics conditions we also expect a rather small contributions from fracture functions. Therefore the central term, $d\sigma^{H,C,(1)}$, can be used to estimate the single parton scattering contribution to the process. The latter might be considered as the baseline to study the contributions of double (or multiple) parton scattering contributions to the same final state, where, for example, the primary scatter produces a Drell-Yan pair while the secondary one produces the detected hadron H .

IV. CONCLUSIONS

We have briefly reviewed a perturbative approach to single particle production associated with a Drell-Yan pair in hadronic collisions. On the theoretical side we have shown that the introduction of fracture functions allows a consistent factorisation of new class of collinear singularities arising in this type of processes. The factorisation procedure coincides with the one used in DIS confirming, as expected, the universal structure of collinear singularities and supports the proposed collinear factorisation formula. On the phenomenological side we have outlined some areas in which the formalism can be fully tested. In particular, focusing on the AFTER@LHC kinematic range, we have discussed in some detail the single diffractive production of virtual photons. The study of such a process might improve our understanding of non-perturbative aspects of QCD and it allows to explore in detail the nature of factorisation breaking at intermediate energies.

-
- [1] M. Basile *et al.*, *Nuovo Cim.* **A66** (1981) 129.
 - [2] J. C. Collins, *Phys. Rev.* **D57** (1998) 3051; *Phys. Rev.* **D61** (2000) 019902 (E);
J. Phys. **G28** (2002) 1069.
 - [3] M. Grazzini, L. Trentadue and G. Veneziano, *Nucl. Phys.* **B519** (1998) 394.
 - [4] L. Trentadue and G. Veneziano, *Phys. Lett.* **B323** (1994) 201.
 - [5] H1 Collaboration, *Eur. Phys. J.* **C48** (2006) 715.
 - [6] H1 Collaboration, *JHEP* (2007) 0710:042.

- [7] ZEUS Collaboration, *Nucl. Phys.* **B831** (2010) 1.
- [8] F. A. Ceccopieri and L. Favart, e-Print: arXiv:1205.6356, e-Print: arXiv:1110.4829.
- [9] F. A. Ceccopieri, *Eur. Phys. J.* **C74** (2014) 3029.
- [10] F. A. Ceccopieri and D. Mancusi, *Eur. Phys. J.* **C73** (2013) 2435.
- [11] A. Berera and D. E. Soper, *Phys. Rev.* **D50** (1994) 4328.
- [12] J. C. Collins *et al.*, *Phys. Lett.* **B307** (1993) 161.
- [13] CDF Collaboration, *Phys. Rev. Lett.* **84** (2000) 5043.
- [14] CDF Collaboration, *Phys. Rev.* **D82** (2010) 112004.
- [15] S. J. Brodsky *et al.*, *Phys. Rept.* **522** (2013) 239 .
- [16] F. A. Ceccopieri, L. Trentadue, *Phys. Lett.* **B668** (2008) 319.
- [17] F. A. Ceccopieri, *Phys. Lett.* **B703** (2011) 491.
- [18] G. Altarelli *et al.*, *Nucl. Phys.* **B157** (1979) 461.
- [19] D. Graudenz, *Nucl. Phys.* **B432** (1994) 351.
- [20] M. Klasen, G. Kramer, *Phys. Rev.* **D80** (2009) 074006.
- [21] G. Camici, M. Grazzini, L. Trentadue, *Phys. Lett.* **B439** (1998) 382 .
- [22] F. A. Ceccopieri, L. Trentadue, *Phys. Lett.* **B655** (2007) 15 .
- [23] A. D. Martin *et al.*, *Phys. Lett.* **B531** (2002) 216.
- [24] CDF Collaboration, *Phys. Rev.* **D65** (2002) 092002.
- [25] CDF Collaboration, *Phys. Rev.* **D82** (2010) 034001.